Archives of Materials Science and Engineering

Volume 112
Issue 1
November 2021
Pages 13-22

International Scientific Journal
published monthly by the
World Academy of Materials
and Manufacturing Engineering

DOI: 10.5604/01.3001.0015.5928

Optimizing the mechanical properties of 3D-printed PLA-graphene composite using response surface methodology

A. El Magri *, S. Vaudreuil
Euromed Polytechnic School, Euromed Research Center, Euromed University of Fes, Meknes road, Bensouda roundabout, 30 000, Fès, Morocco
* Corresponding e-mail address: a.elmagri@ueuromed.org
ORCID identifier: https://orcid.org/0000-0003-2376-0814 (A.E.M.)

ABSTRACT

Purpose: This work aims to study the relationship between various processing parameters to fabricate PLA-graphene based 3D parts with high mechanical properties. The selected parameters in this study are known for their critical impact on the final properties of printed parts.

Design/methodology/approach: Three key printing parameters are simultaneously studied in a systematic manner using central composite design (CCD). The selected printing parameters are printing temperature, printing speed, and layer thickness.

Findings: Through a variance analysis, all tested printing parameters significantly impact the final properties of printed PLA-graphene's parts. A response surface methodology (RSM) was also applied to analyse the results and to optimize the tensile and the flexural properties. According to this latter methodology, the optimum factor levels are found at 200°C printing temperature, 34.65 mm s^{-1} printing speed and 0.2 mm layer thickness.

Research limitations/implications: Results indicate that layer thickness and printing speed are the dominant contributors to tensile and flexural properties.

Originality/value: As one of the few polymers loaded with nanoparticles available, polylactic acid (PLA) reinforced graphene was selected in this study as a base material for FFF 3D printing process. A response surface methodology was applied to analyse the results and to maximize the tensile and flexural properties of 3D printed PLA-graphene composite.

Keywords: PLA, Graphene, Composite, Fused filament fabrication, Response surface methodology, Mechanical properties

Reference to this paper should be given in the following way:

A. El Magri, S. Vaudreuil, Optimizing the mechanical properties of 3D-printed PLA-graphene composite using response surface methodology, Archives of Materials Science and Engineering 112/1 (2021) 13-22. DOI: https://doi.org/10.5604/01.3001.0015.5928

MATERIALS MANUFACTURING AND PROCESSING

© Copyright by International OCSCO World Press. All rights reserved. 2021

1. Introduction

Additive manufacturing (AM) is a family of processes enabling the layer upon layer production of an object from three-dimensional (3D) model data. This process has shown significant potential and alternative methods to process materials for use in different industries. One of the many benefits of AM is the production of functional parts with complex geometries that are difficult to manufacture by subtractive manufacturing methodologies [1-3].

Thanks to its ease of use and lower investment and operating costs, Fused Filament Fabrication (FFF) is an extensively used AM technologies [4,5]. In this method, the thermoplastic filament is fed into a heated nozzle, melted and subsequently extruded and deposited layer by layer onto a build plate forming the desired 3D part. Various thermoplastics are currently used to produce parts satisfactorily by FFF. Among them are polylactic acid (PLA), acrylonitrile butadiene styrene (ABS), polycarbonate (PC), PC-ABS blends and polyphenyl sulfone (PPSF) [6-8]. Parts printed with these thermoplastic usually exhibits low physical properties, limiting their use in engineering applications. To overcome this problem, the addition of fibres or fillers in the polymer matrix could increase the mechanical and thermal properties to levels sufficient for new applications [9]. Chasemi and al [10] investigated the reinforcing effects of a hybrid filler, including talc and exfoliated graphene nanoplatelets (xGnPs), in poly-propylene (PP) composites. From the analysis of variance (ANOVA), it was found that the talc and xGnP play a significant role in the mechanical properties and morphology of the composites.

In the FFF process, multiple controllable printing parameters, such as printing speed, printing temperature, raster angle and layer thickness, are accounted to produce high qualified 3D-printed parts. Chieng et al [11] have employed the response surface methodology (RSM) coupled with central composite design (CCD) to optimize the tensile strength of poly(lactic acid) (PLA)/graphene nano-composites. Results showed that graphene loading and printing temperature had a significant effect on tensile strength response. Most studies reported the dependence between the mechanical properties and the selected printing parameters [5,12,13]. El Magri and al. investigated the effect of nozzle temperature and infill orientation on tensile properties and crystallinity of 3D-printed virgin polylactic acid (PLA) and short carbon fibre (CF)-reinforced PLA. For both materials, the maximum tensile properties have attained for 230°C nozzle temperature and [0/15/-15°] infill orientation. In another study, researchers found that the nozzle temperature, printing speed, raster angle and layer thickness parameters need to be taken into serious consideration. They found that these printing parameters directly impact the tensile properties and crystallinity of FFF printed materials [1,7,14].

Graphene's addition to polymer matrices is currently under investigation as a promising method to improve their service conditions. Graphene's excellent mechanical, electrical and thermal properties make it an excellent candidate for the reinforcement of several polymers [15]. Recently, PLA-polymer-graphene nanocomposites have been 3D-printed due to the attractive features of both materials. However, in composites, the main challenge is to understand the graphene's properties transfer from the nanoscale to the macroscale. Caminero and al [15] reported that the printed samples based PLA-Graphene composite samples showed the best performance in terms of surface texture, tensile and flexural stress than un-reinforced PLA. However, the impact strength of the PLA-Graphene composite samples has been reduced by 1.2-1.3 times when compared with un-reinforced PLA. By using central composite design, Camargo and al. [16] studied the effect of the variation of the infill and layer thickness parameters on the mechanical properties of 3D-printed PLA-graphene. The results showed that the mechanical properties increase by increasing the layer thickness and infill density parameters, while impact energy decreased as the infill increased.

Previous studies have shown the possibility of printing PLA-Graphene by FFF, but few of them have investigated the influence and the optimization of process parameters on the mechanical properties of the printed parts. For this purpose, three key printing parameters were selected; printing temperature, printing speed and layer thickness to analyse their impact on the mechanical properties of additively manufactured PLA-graphene's parts. Central composite design (CCD), was used to minimize the number of experiments, which were then processed by the response surface methodology (RSM) to determine the optimum combination of factor ranges.

2. Material and specimens fabrication

The polylactic acid plastic reinforced graphene (PLA-graphene) filament used in this work was purchased from SynerG Haydale (United Kingdom) with a graphene content of 0.5 wt.%. This filament has a diameter of 1.75 ± 0.02 mm, a density of 1.24 g cm^{-3} and a glass transition temperature of 67°C. The filament was dried for 4 hours at 60°C prior to printing. An INTAMSYS (Intelligent Additive Manufacturing Systems) FunMAT HT was used for processing PLA-Graphene. This FFF system, equipped with both a heated

Table1.
Fused filament fabrication printing parameters

Printing parameters	Value	Unit
Printing temperature	190 to 240	°C
Printing speed	20 to 50	mm s^{-1}
Bed temperature	50	°C
Infill line directions [*relative to the long axis of the test bar*]	[45/-45]	°
Layer height	0.1 to 0.30	mm
Infill pattern	Lines	
Line width	0.4	mm
Infill density	100	%
Number of bottom / top layers	2/2	layer
Number of contours	2	wall

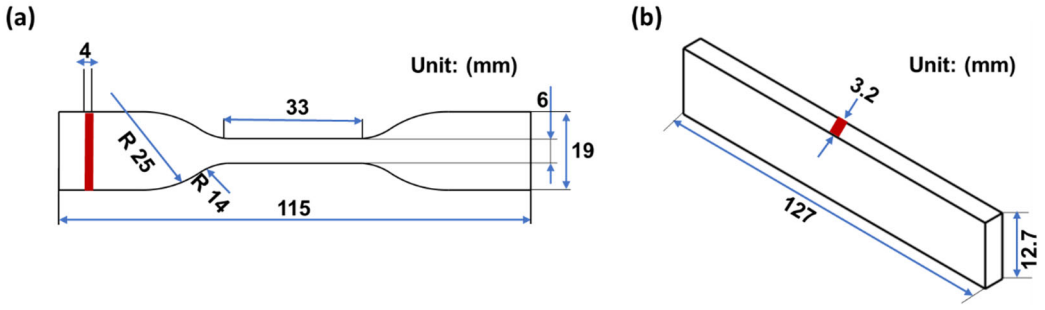

Fig. 1. a) Tensile test bar dimensions, b) flexural test bar dimensions

bed and a build chamber, has a build volume of 260 x 260 x 260 mm. Tensile and flexural test specimens were printed directly on the heated glass bed for good first layer adhesion. The infill parameter was set to 100% to obtain solid-like samples. The major printing parameters evaluated are summarized in Table 1. All specimens were printed flat on the build platform (XY surface). Slicing of the 3D-model into individual layers was performed using the INTAM-suite software v3.5.2.

3. Mechanical testing

Tensile testing was performed following ASTM D638-14 "Standard Test Method for Tensile Properties of Plastics" and according to the ASTM D790-02 ''Flexural Properties of Unreinforced and Reinforced Plastics and Electrical Insulating Materials'' for flexural testing. A Criterion C45.105 electromechanical universal testing machine (MTS, USA) equipped with a 10 kN load cell and self-tightening jaws was used for testing at a crosshead displacement speed of 5 mm min^{-1}. The flexural tests were performed on the same machine, using the 3-point bending fixture with the push down speed of 5 mm min^{-1}. Flexural tests were carried out with a span length of 50 mm. The shape and dimensions of the specimens were defined in accordance with the standards (Figs. 1 (a) and (b)) as above mentioned, and six samples of each series were manufactured.

4. Design of experiments

Design of experiments (DOE) is a powerful tool for analysing the influence of process variables on specified properties. For this purpose, central composite design (CCD) was used as DOE method in this work to determine the number of experiments to be evaluated for the optimization of three printing parameters namely printing temperature (T), printing speed (S), and layer thickness (L) and three responses namely Young's modulus (E), tensile strength (σ_t), and flexural strength (σ_f).

Based on the CCD, the correlation between tested experimental factors (T, S, and L) and measured response (E, σ_t and σ_f) is evaluated by response surface methodology (RSM). The experimental data can be fitted using a second-

order polynomial response surface model as expressed in Eq. (1).

$$Y = \beta_0 + \sum_{i=1}^{N} \beta_i X_i + \sum_{i=1}^{N} \beta_{ii} {X_i}^2 + \sum_{i \neq j}^{N} \beta_{ij} X_i X_j + \varepsilon \quad (1)$$

where Y is the predicted response (E, σ_t and σ_f), β_0, β_i , β_{ii}, β_{ij} represent the regression coefficients for the intercept, linear, quadratic and interaction terms, respectively. X_i and X_j represent the coded printing parameters (T, S, and L).The experimental error is represented by ε.

The ranges of the applied parameters for the CCD are represented in Table 2. Level limits have been selected according to observations in a preliminary experimental phase. This phase yielded values of printing temperature ranges in the [190-240°C] range, printing speed in the [20-50 mm s^{-1}] range and layer thickness in the [0.1-0.3 mm] range. The printing parameters are presented into three levels (low, basal and high) with coded value (-1,0,1) and the starting points of ± 1.68 for ± α in the CCD pattern.

The statistical software Minitab version 18 (USA) was used in this study for the DOE to generate the statistical model and plot the response surface for parameters optimization. ANOVA is also used to develop the regression model and to assess the effect of each parameter on the mechanical properties.

5. Results and discussion

5.1. Tensile and flexural properties

The mechanical properties were evaluated for multiple processing parameters at various levels to examine their influence on Young's modulus, tensile strength and flexural strength. All specimens were printed according to [0/15/-15°] orientations relative to the long axis of the test bar to reduce layer delamination [14,17]. Figure 2 shows the typical tensile stress-strain curves of all printed parts according to the various printing conditions. All tested specimens exhibiting a maximum in the stress/strain curve followed by yielding deformation. Printed PLA-graphene samples display necking behaviour. Yield points in this case associated with a deformation mechanism which absorbs energy.

Table 2.
Tested ranges of the applied printing parameters for the CDD

Factor	Code	Level					Unit
		-1.68	-1	0	+1	+1.68	
Printing temperature	T	190	200	215	230	240	°C
Printing speed	S	20	26	35	43	50	mm s^{-1}
Layer thickness	L	0.10	0.14	0.20	0.26	0.30	mm

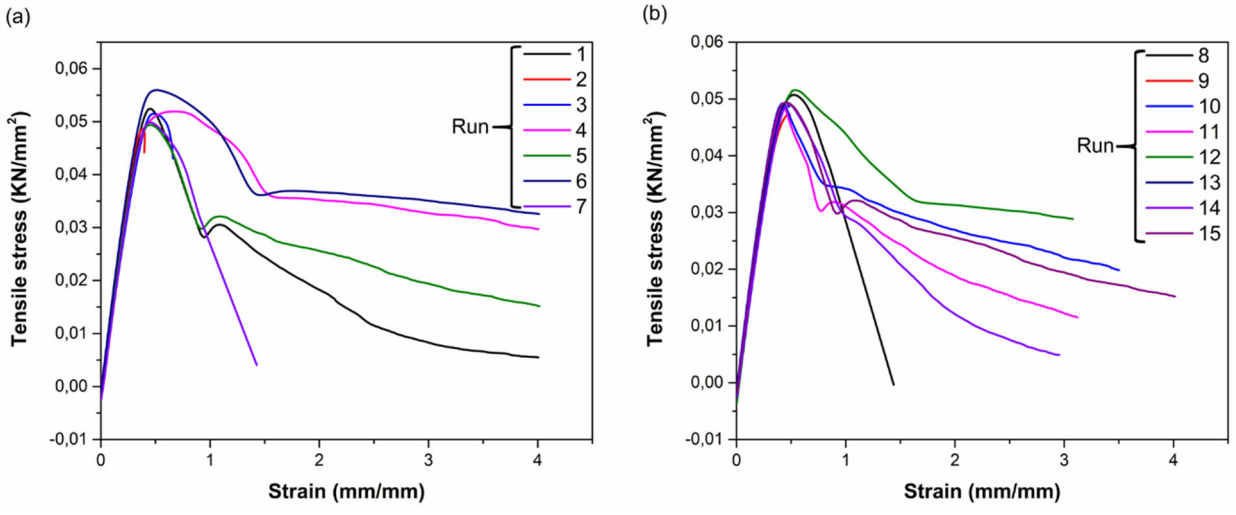

Fig. 2. Stress-strain curves of printed PLA-graphene in different conditions according to DOE

Table 3 summarizes the mechanical properties of PLA-graphene test specimens printed under various printing conditions. This table shows the impact of combined factors on mechanical properties. The highest elastic modulus is recorded for printing conditions of 34.6 mm s^{-1} printing speed, layer thickness of 0.2 mm and 215 and 240°C printing temperatures. At 200°C printing temperature and 0.26 mm layer thickness, 43.3 and 26 mm s^{-1} printing speed yield parts with the highest tensile and flexural strength respectively.

5.2. Analysis of variance (ANOVA) and RSM model fitting

The impact of printing parameters (*T, S,* and *L*) on various response parameters are determined using analysis of variance (ANOVA). The statistical significance of parameters was defined by the probability p-value that should be lower than the alpha value set to 0.05. To verify the performance of the models, an ANOVA analysis was applied for analysing the result of a full quadratic model by calculating their p-value and their R-squared values. The Pareto charts indicate the main and interaction effects generated by ANOVA. They have also the advantage to identify the standardized effects of different linear, quadratic and interacted terms of *T, S,* and *L* versus the corresponding standard value of 1.530 (see Fig. 3). Any effects exceeding this line (1.530) are considered significant in the model. The regression models of selected responses were established from the response surface methodology (RSM). Printing temperature (*T*), printing speed (*S*) and layer thickness (*L*) have been considered as the printing parameters while Young's modulus (E), tensile strength (σ_t), and flexural strength (σ_f) are taken as measured responses. The results can be expressed as a function of printing parameters as follows:

$$y_i = f_p(Tn_{ip}, Sp_{ip}) + \varepsilon_{ip} \quad (2)$$

where y_i is the response, ε the residual and p the number of observations in a factorial experiment.

The Pareto chart (Fig. 3a) for Young's modulus response indicates clearly that the quadratic effects of layer thickness parameter ($L \times L$) and printing speed ($S \times S$) are significant with p-value of 0.003 and 0.020 respectively. The printing temperature (*T*) is no significant parameter in Young's Modulus model. At the opposite, the interaction $T \times L$ is significant in the model with a p-value of 0.094. The less significant parameter in this predictive model is the layer thickness (*L*) in its quadratic form with a p-value of 0.126. If the tensile strength response is evaluated (Fig. 3b), the quadratic effect of printing speed ($S \times S$) is the most significant parameter (p-value = 0.001) followed by its linear effect with a p-value of 0.018. Layer thickness and printing

Table 3.
Experimental results according to DOE

	Factor			Response		
# Run	*T*, °C	*L*, mm	*S*, mm s^{-1}	Young modulus, MPa	Tensile strength, MPa	Flexural strength, MPa
1	215.0	0.10	34.6	3237 ± 20	54.3 ± 1.1	93.0 ± 1.5
2	215.0	0.20	34.6	3532 ± 22	54.8 ± 1.2	98.3 ± 1.6
3	215.0	0.30	34.6	2965 ± 23	49.4 ± 1.1	89.2 ± 1.4
4	200.2	0.26	43.3	3152 ± 21	50.7 ± 1.1	93.5 ± 1.5
5	200.2	0.26	26.0	3326 ± 26	47.7 ± 1.2	100.0 ± 1.6
6	240.0	0.20	34.6	3532 ± 23	54.8 ± 1.3	98.3 ± 1.4
7	200.2	0.14	43.3	3337 ± 27	54.0 ± 1.4	97.4 ± 1.3
8	229.9	0.14	26.0	3221 ± 19	42.3 ± 1.1	92.1 ± 1.5
9	229.9	0.26	43.3	2529 ± 24	50.3 ± 1.2	87.7 ± 1.2
10	229.9	0.26	26.0	2762 ± 28	43.9 ± .11	94.5 ± 1.4
11	190.1	0.20	34.6	3403 ± 35	49.2 ± 1.0	97.4 ± 1.4
12	215.0	0.20	49.1	3402 ± 33	49.0 ± 1.1	93.0 ± 1.3
13	200.2	0.14	26.0	3007 ± 21	48.6 ± 1.2	88.7 ± 1.2
14	215.0	0.20	20.1	3082 ± 20	46.6 ± 1.1	89.6 ± 1.5
15	229.9	0.14	43.3	2972 ± 22	48.9 ± 1.0	84.5 ± 1.2

temperature parameters are significant only in their quadratic forms with a p-value of 0.050 and 0.056 respectively.

For the flexural strength response (Fig. 3c), the quadratic effects of layer thickness ($L \times L$) and printing speed (S×S) terms are more significant in the flexural strength model with a p-values of 0.005 and 0.007 respectively, followed by the interactions $T \times S$ and $L \times S$ with p-values of 0.079 and 0.122 respectively. As the printing temperature term exceeded the 1.530, and its p-value is superior to 0.05, it can be considered as less significant in the flexural strength model's.

To verify the performance of the models, an ANOVA analysis was applied for analysing the result of the full quadratic models by calculating their R-squared values, relative error (RE) values for each model and their p-values. As discussed above, if the p value of the term is lower than 0.05, this coefficient is considered in the final model.

In this work, we have correlated the values of responses with the selected printing parameters using multiple linear regression techniques. By using stepwise forward and backward linear regression analysis, their standard deviations and the variance of each model have been determined. The suggested empirical models developed for each output response (E, σ_t and σ_f) are listed in Table 4.

As presented in Table 4, all regression models exhibit a low relative error RE (< 10 %) and a significant probability value (p-value <0.05). Based on these results, all regression models were chosen to predict the mechanical responses. As can be seen in Table 4, the coefficient of determination R^2

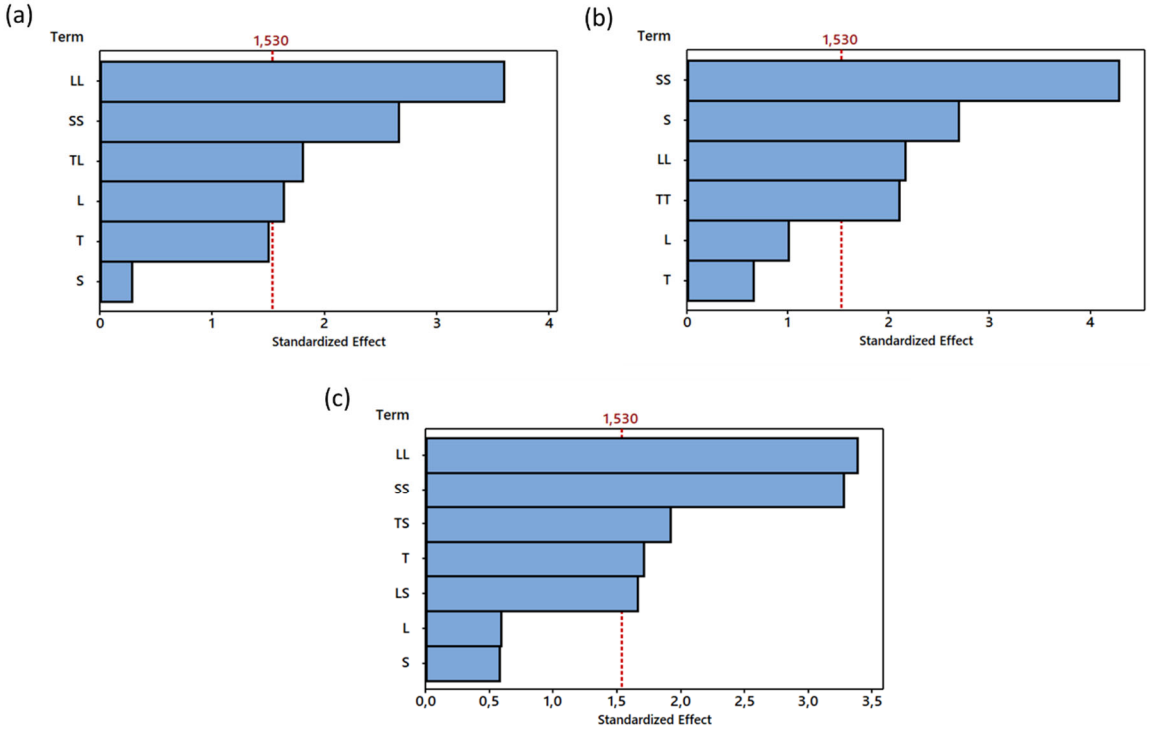

Fig. 3. Pareto chart of the standardized effects of (a) Young's modulus, (b) tensile strength and (c) flexural strength

Table 4.
RSM predictive regression models

Response	RSM Model	R^2	RE	P-value
Young's modulus, MPa	$E = -6197 + 51957 \times L - 53079 \times L^2 - 1.888 \times S^2 - 145.4 \times T \times L$	0.672	3.2%	0.012
Tensile strength, MPa	$\sigma_t = -305 + 2.888 \times S - 0.00644 \times T^2 - 405 \times L^2 - 0.03856 \times S^2$	0.713	2.9%	0.005
Flexural strength, MPa	$\sigma_f = -101.0 + 0.463 \times T - 750 \times L^2 - 0.0350 \times S^2 - 0.01611 \times T \times S - 3.45 \times L \times S$	0.717	2.9%	0.013

of E was found to be around 0.672, meaning that 67.2% of the variation in printing temperature, printing speed and layer thickness fits within the Young's modulus model with a p-value of 0.012. This means that Young's modulus model can be applied to the data correctly. It can be seen that this response (E) is highly dependent on layer thickness (L) while being independent on printing speed and printing temperature, which are not considered significant in this case (p-value > 0.05). Contrariwise, the interaction temperature layer thickness is significant. In this case, for a given polymer layer thickness, the nozzle temperature is responsible for the molecular chains order and the generation of crystalline regions which directly impact the elastic property of the manufactured polymer by FFF process [1,5].

The regression model of tensile strength (σ_t) shows a p-value of 0.005 and a R^2 greater than 71% which indicate that the model applies to a high degree of accuracy compared to Young's modulus model. It can be concluded that the σ_t is mainly affected by printing speed with a probability value of 0.018. The printing temperature and layer thickness are insignificant terms in this case (p-value > 0.05). Thus, maximizing the tensile strength property of printed PLA-graphene by FFF requires a higher printing speed. Printing with high speed in the acceptable range may reduce the extrusion defects and intensify the density of printed filaments [14]. The extrusion speed impacts the melt pressure of the polymer in the printer nozzle which consequently, affects the surface morphology and extrusion width of the extruded filament through the nozzle. At a lower extrusion speed, expansion of the molten polymer is a predominant mechanism of the molten polymer extruded through the printer nozzle. Generally, high printing speed generates higher melt pressure in the nozzle which is beneficial to reducing surface defects of the extruded polymer [18].

The predictive flexural strength model (σ_f) in Table 4 represents the quadratic terms of layer thickness and printing speed, the linear terms of printing temperature and the interaction terms printing speed and the quadratic effects of printing temperature. The interaction terms of the printing temperature and speed with layer thickness are significant in this model. ANOVA results show that $L \times L$ and $S \times S$ are more significant model terms for flexural strength with p-value of 0.005 and 0.007 respectively. The high value of R^2 (71.7%) with a model's p-value of 0.013, indicating that the predicted values can thus be considered in good accordance with experimental values. From this mathematical model, the response variable (σ_f) increases by increasing printing temperature and decreasing layer thickness. Increasing printing temperature from 190 to 240°C promotes a decrease of the PLA melt viscosity. This improves the diffusion of newly extruded PLA molecules in the underlying layer to help create a stronger interlayer adhesion and consequently, high flexural strength [19].

5.3. Responses optimization

The main objective of RSM is the determination of the optimum conditions of FFF printing parameters that maximize all responses to obtain 3D-printed PLA-graphene composite with high mechanical performance. Three-dimensional response surface was presented as graphical representations of the regression model to determine the optimum values of responses and to achieve a better understanding of the interaction between printing parameters. The predicted results of three-dimensional Young's modulus, tensile strength and flexural strength as response surfaces variable for the printing temperature and layer thickness variables are shown in Figure 4. The printing speed was holding at 34.65 mm s^{-1}, because the maximum levels of responses were achieved at this value. As showed in the Figure 4, all response surfaces are curved, this confirm that the predicted models in these cases contain quadratic and interaction terms that are statistically significant.

Based on the predictive model of each response a graphical of multi-response optimization technique was implemented to determine the best combination of printing parameters that maximize as much as possible tensile and flexural properties.

Overlaid contour plot was used to identify the optimal area where the predicted means of all response variables are in an acceptable range [20]. This feasible region is an area that is formed by printing temperature and layer thickness variables, given the holding values to printing speed (34.65 mm s^{-1}), such that the fitted values for each response are between their respective contours. Each set of contours defines the boundaries of acceptable values of the fitted response. The solid contour is defined as the lower limit and the dotted contour is the upper limit of each mechanical property. The contours of each response are displayed in a different colour (see Fig. 5). The overlaid contour plots were used in this study to identify an area of compromise among all responses, to find a setting range for each printing parameter yielding high tensile and flexural properties of 3D printed PLA-graphene composite. Figure 5 shows the contour plot of all superimposed responses and the optimal region (white region) that satisfies all response criteria imposed. The criteria used for constraint optimization were: flexural strength ($96 < \sigma_f < 100$ MPa), tensile strength ($53 < \sigma_t < 54.3$ MPa) and Young's modulus ($3510 < E < 3550$ MPa).

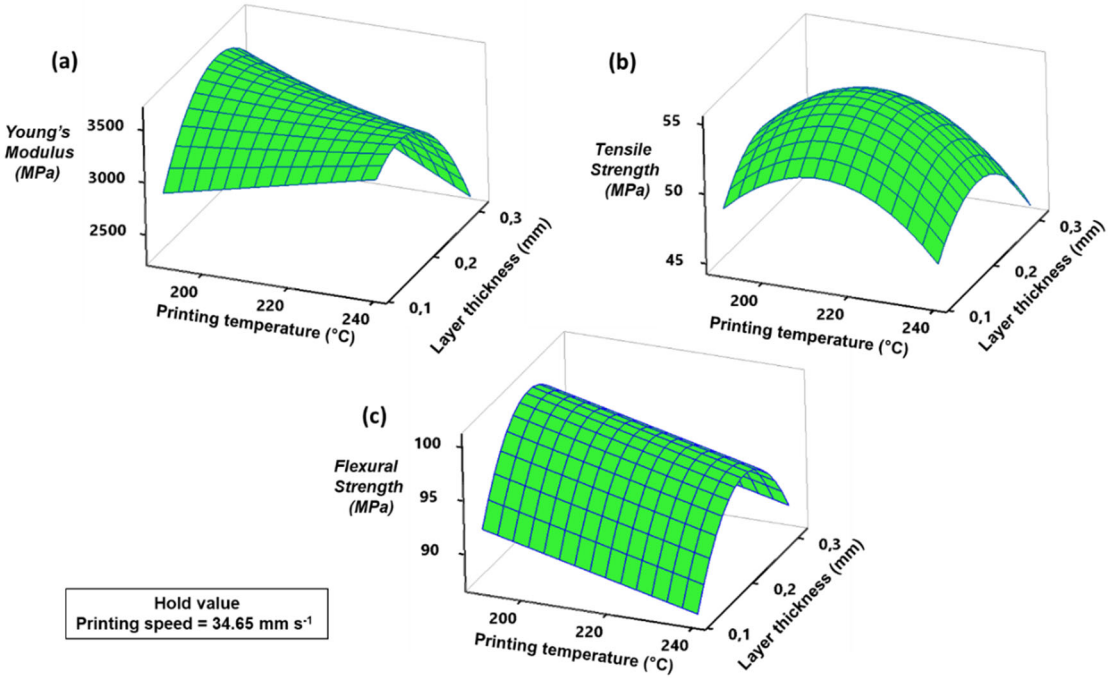

Fig. 4. Response surface of: (a) Young's modulus, (b) tensile strength and (c) flexural strength as a function of printing temperature and layer thickness

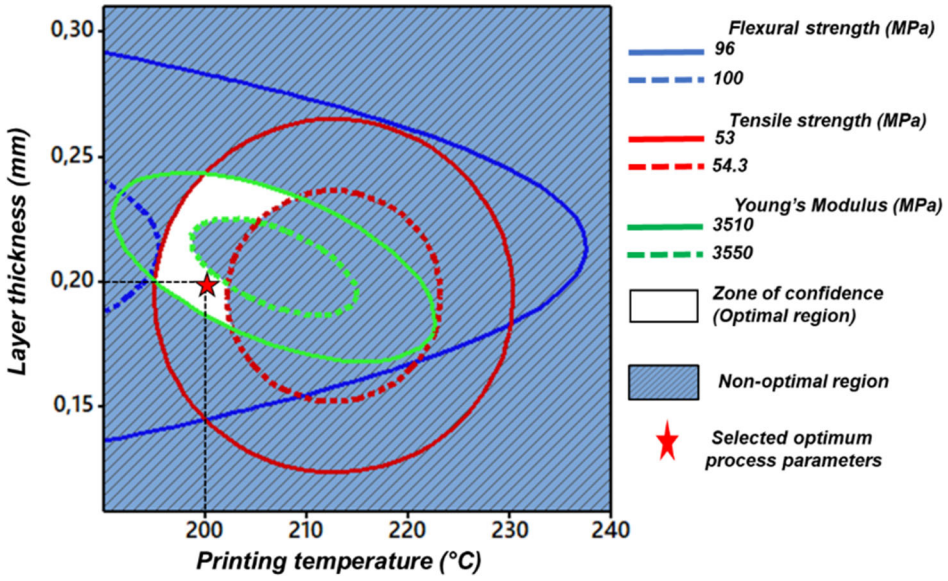

Fig. 5. Graphical multi-response optimization

The superimposed contour plot exhibits an optimal area where all criteria are met. From this plot, the optimum printing parameters found for a printing speed of 34.65 mm s^{-1} are a printing temperature of 200°C and a 0.2 mm layer thickness. Printed specimens according to these optimums printing parameters show good accordance with the imposed criteria. The obtained results are 3560 ± 40 MPa, 54.7 ± 1.3 MPa and 98.9 ± 1.4 MPa for

Young's modulus, tensile strength and the flexural strength respectively.

6. Conclusions

The aim of this present work was to study the impacts of three key FFF printing parameters on the mechanical properties of PLA-graphene composite parts. The selected printing parameters are known for their critical impact on the final performances of 3D-printed parts. These parameters are printing temperature, printing speed, and layer thickness. To study the significance of each parameter while minimizing the number of required experiments, a Central Composite Design (CCD) approach was used.

The statistical significance of each parameter was defined through the Analysis of Variance (ANOVA). Results indicate that layer thickness and printing speed are the dominant contributors to tensile and flexural properties. A surface response methodology (RSM) was used afterward to optimize the responses for the provided input factors, leading to establish optimum levels of printing temperature, printing speed, and layer thickness. According to RSM, the optimum factor levels which maximize all output responses are 200°C for printing temperature, 34.65 mm s^{-1} for printing speed and 0.2 mm for layer thickness.

Acknowledgements

The authors also gratefully acknowledge the support from Euromed University of Fes (UEMF), and the financial contribution of the Hassan II Academy of Sciences and Technology and of Safran Composites.

References

[1] A. El Magri, S. Vaudreuil, K. El Mabrouk, M. Ebn Touhami, Printing temperature effects on the structural and mechanical performances of 3D printed poly-(phenylene sulfide) material, IOP Conference Series: Materials Science and Engineering 783 (2020) 012001. DOI: https://doi.org/10.1088/1757-899X/783/1/012001

[2] M. Mansour, K. Tsongas, D. Tzetzis, Measurement of the mechanical and dynamic properties of 3D printed polylactic acid reinforced with graphene, Polymer-Plastics Technology and Materials 58/11 (2019) 1234-1244.
DOI: https://doi.org/10.1080/03602559.2018.1542730

[3] Y. Li, Z. Feng, L. Huang, K. Essa, E. Bilotti, H. Zhang, T. Peijs, L. Hao, Additive manufacturing high performance graphene-based composites: A review, Composites Part A: Applied Science and Manufacturing 124 (2019) 105483. DOI: https://doi.org/10.1016/j.compositesa.2019.105483

[4] J. Martínez, J.L. Diéguez, E. Ares, A. Pereira, P. Hernandez, J.A. Pérez, Comparative between FEM models for FDM parts and their approach to a real mechanical behaviour, Procedia Engineering 63 (2013) 878-884.
DOI: https://doi.org/10.1016/j.proeng.2013.08.230

[5] A. El Magri, S. Vanaei, S. Vaudreuil, An overview on the influence of process parameters through the characteristic of 3D-printed PEEK and PEI parts, High Performance Polymers 33/8 (2021) 862-880. DOI: https://doi.org/10.1177/09540083211009961

[6] O.A. Mohamed, S.H. Masood, J.L. Bhowmik, Optimization of fused deposition modeling process parameters: a review of current research and future prospects, Advances in Manufacturing 3 (2015) 42-53. DOI: https://doi.org/10.1007/s40436-014-0097-7

[7] A. El Magri, K. El Mabrouk, S. Vaudreuil, M. Ebn Touhami, Experimental investigation and optimization of printing parameters of 3D-printed polyphenylene sulfide through response surface methodology, Journal of Applied Polymer Science 138/1 (2020) 49625. DOI: https://doi.org/10.1002/app.49625

[8] H. Vanaei, M. Shirinbayan, M. Deligant, K. Raissi, J. Fitoussi, S. Khelladi, A. Tcharkhtchi, Influence of process parameters on thermal and mechanical properties of polylactic acid fabricated by fused filament fabrication, Polymer Engineering and Science 60/8 (2020) 1822-1831.
DOI: https://doi.org/10.1002/pen.25419

[9] N.G. Karsli, A. Aytac, Tensile and thermomechanical properties of short carbon fiber reinforced polyamide 6 composites, Composites Part B: Engineering 51 (2013) 270-275.
DOI: https://doi.org/10.1016/j.compositesb.2013.03.023

[10] F. Ashenai Ghasemi, I. Ghasemi, S. Menbari, M. Ayaz, A. Ashori, Optimization of mechanical properties of polypropylene/talc/graphene composites using response surface methodology, Polymer Testing 25 (2016) 283-292. DOI: https://doi.org/10.1016/j.polymertesting.2016.06.012

[11] B.W. Chieng, N.A. Ibrahim, W.M.Z. Wan Yunus, Optimization of Tensile Strength of Poly(Lactic Acid)/Graphene Nanocomposites Using Response Surface Methodology, Polymer-Plastics Technology and Engineering 51/8 (2012) 791-799. DOI: https://doi.org/10.1080/03602559.2012.663043

[12] H.R. Vanaei, M. Deligant, M. Shirinbayan, K. Raissi, J. Fitoussi, S. Khelladi, A. Tcharkhtchi, A comparative in-process monitoring of temperature profile in fused filament fabrication, Polymer Engineering and Science 61/1 (2021) 68-76. DOI: https://doi.org/10.1002/pen.25555

[13] A. El Magri, K. El Mabrouk, S. Vaudreuil, Preparation and characterization of poly(ether ether ketone)/ poly(ether imide) [PEEK/PEI] blends for fused filament fabrication, Journal of Materials Science 56 (2021) 14348-14367. DOI: https://doi.org/10.1007/s10853-021-06172-x

[14] A. El Magri, K. El Mabrouk, S. Vaudreuil, H. Chibane, M. Ebn Touhami, Optimization of printing parameters for improvement of mechanical and thermal performances of 3D printed poly(ether ether ketone) parts, Journal of Applied Polymer Science 137/37 (2020) 49087. DOI: https://doi.org/10.1002/app.49087

[15] M.Á. Caminero, J.M. Chacón, E. García-Plaza, P.J. Núñez, J.M. Reverte, J.P. Becar, Additive Manufacturing of PLA-Based Composites Using Fused Filament Fabrication: Effect of Graphene Nanoplatelet Reinforcement on Mechanical Properties, Dimensional Accuracy and Texture, Polymers 11/5 (2019) 799. DOI: https://doi.org/10.3390/polym11050799

[16] J.C. Camargo, Á.R. Machado, E.C. Almeida, E.F.M.S. Silva, Mechanical properties of PLA-graphene filament for FDM 3D printing, The International Journal of Advanced Manufacturing Technology 103 (2019) 2423-2443. DOI: https://doi.org/10.1007/s00170-019-03532-5

[17] A. El Magri, K. El Mabrouk, S. Vaudreuil, M. Ebn Touhami, Mechanical properties of CF-reinforced PLA parts manufactured by fused deposition modeling, Journal of Thermoplastic Composite Materials 34/5 (2021) 581-595. DOI: https://doi.org/10.1177/0892705719847244

[18] P. Geng, J. Zhao, W. Wu, W. Ye, Y. Wang, S. Wang, S. Zhang, Effects of extrusion speed and printing speed on the 3D printing stability of extruded PEEK filament, Journal of Manufacturing Processes 37 (2019) 266-273. DOI: https://doi.org/10.1016/j.jmapro.2018.11.023

[19] V. Kishore, X. Chen, C. Ajinjeru, A.A. Hassen, J. Lindahl, J. Failla, V. Kunc, C. Duty, Additive Manufacturing of High Performance Semicrystalline Thermoplastics and Their Composites, Proceedings of the 27th Annual International Solid Freeform Fabrication Symposium, Austin, Texas, USA, 2016, 906-915.

[20] Minitab 18 Support. Avaliable from: https://support.minitab.com/en-us/minitab/18/, Access in: 10.04.2021.

Creative Commons Attribution-NonCommercial-NoDerivatives International 4.0 BY NC ND

© 2021 by the authors. Licensee International OCSCO World Press, Gliwice, Poland. This paper is an open access paper distributed under the terms and conditions of the Creative Commons Attribution-NonCommercial-NoDerivatives 4.0 International (CC BY-NC-ND 4.0) license (https://creativecommons.org/licenses/by-nc-nd/4.0/deed.en).